catalysts

MDPI

Article

Fe-Ni Bimetallic Modified HZSM-5 for Efficient Preparation of Monocyclic Aromatic Hydrocarbons via Co-Pyrolysis of PET and LDPE

Haijian Yang [1], Changsen Zhang [2,*], Lianfeng Shang [1], Hanfang Feng [1] and Na Xiao [1]

[1] Faculty of Engineering, Huanghe Science and Technology University, Zhengzhou 450063, China; yanghj@hhstu.edu.cn (H.Y.); shanglf@hhstu.edu.cn (L.S.); fenghf@hhstu.edu.cn (H.F.); 201608156@hhstu.edu.cn (N.X.)
[2] School of Ecology and Environment, Zhengzhou University, Zhengzhou 450001, China
* Correspondence: zhangcs@zzu.edu.cn

Abstract

Plastic waste has become a serious global issue. Thermal treatment of waste PET faces critical drawbacks including severe reactor clogging and low-value oxygen-rich bio-oil, restricting large-scale chemical recycling. Co-pyrolysis with hydrogen-rich low-density polyethylene (LDPE) over modified zeolite provides a viable route to overcome these barriers. In this study, reaction parameters including temperature, plastic/catalyst ratio and PET/LDPE ratio were optimized, and Fe-Ni bimetallic modified HZSM-5 was fabricated via impregnation to boost monocyclic aromatic hydrocarbons (MAHs) production. LDPE served as a hydrogen donor to facilitate PET deoxygenation via synergistic effects. At 550 °C with a plastic/catalyst ratio of 1:4 and PET/LDPE ratio of 2:3, the liquid yield hit 80.2%, and all detectable organic compounds in the liquid phase identified by GC–MS were aromatic hydrocarbons. Among all prepared mono- and bimetallic zeolites, 3Fe7Ni/HZ delivered optimal MAHs selectivity at 80.5%. This 20% promotion over unmodified HZSM-5 stems from balanced metal dispersion and tuned acid sites unique to Fe–Ni co-loading. This work offers a feasible strategy for converting waste plastics into high-value aromatics and further trials with varied metal contents will be needed to extend industrial applicability.

Keywords: waste plastics; catalytic pyrolysis; HZSM-5; bimetallic modification; monocyclic aromatic hydrocarbons; deoxygenation and upgrading

1. Introduction

Since its invention in the 1930s, fossil fuel-based plastic products have been widely used worldwide due to their low cost and versatile performance, with their output increasing by 20 times over the past half century [1]. However, the uncontrolled accumulation of plastic waste has posed dual challenges for the ecological environment and energy security. It is estimated that without effective recycling technologies, the global annual plastic output will exceed 500 million tons by 2050, among which more than 80% will end up in landfills or incinerators. Traditional disposal methods have obvious drawbacks: landfilling occupies massive land resources and easily triggers groundwater pollution; incineration emits greenhouse gases and toxic and harmful substances; mechanical recycling is confronted with complex classification, high cost and limited recycled product quality [2,3]. Therefore, developing efficient chemical recycling technologies to directionally convert waste plas-

Check for updates

Academic Editor: Narendra Kumar

Received: 25 June 2026
Revised: 2 August 2026
Accepted: 17 August 2026
Published: 24 August 2026

Copyright: © 2026 by the authors. Licensee MDPI, Basel, Switzerland. This article is an open access article distributed under the terms and conditions of the Creative Commons Attribution (CC BY) license.

tics into fuels and high-value chemicals has become a critical approach to mitigate white pollution and reduce reliance on fossil fuels.

As a promising chemical recycling technology for waste plastics, catalytic pyrolysis can regulate product distribution via catalysts to achieve the targeted synthesis of specific compounds [4]. Aromatic hydrocarbons, especially monocyclic aromatic hydrocarbons (MAHs), such as benzene, toluene and xylene, are core raw materials of the petrochemical industry, which are widely applied in the production of plastics, resins, solvents and other products. Currently, MAHs are mainly derived from petroleum refining, which is restricted by the depletion of fossil energy [5]. As one of the top ten plastics worldwide, PET has an annual production capacity of about 70 million tons, accounting for 12% of solid plastic waste [6]. Its molecular structure contains benzene rings, laying a structural foundation for conversion into aromatic hydrocarbons. Nevertheless, individual pyrolysis of PET has prominent defects: the cleavage of ester bonds generates a large amount of benzoic acid, terephthalic acid and other benzoic acid derivatives, which will block equipment after condensation. In addition, the pyrolysis oil yield is merely about 23%, and nearly half of the components are oxygen-containing aromatic compounds, resulting in strong corrosiveness and low utilization value of the oil product [7,8]. Recent studies have demonstrated that PET can be directly converted into BTX aromatics even without external hydrogen supply by unlocking hidden hydrogen in the polymer structure, providing a new strategy for PET chemical upcycling [9].

Studies have demonstrated that increasing the carbon–hydrogen ratio of reactants is an effective strategy to improve the quality of pyrolysis products from oxygen-containing plastics. As a hydrogen-rich plastic, LDPE produces a large number of olefins and alkanes during pyrolysis. It can serve as a hydrogen donor for PET in co-pyrolysis processes, facilitating deoxygenation via Diels–Alder reactions and raising aromatic hydrocarbon yield [10,11]. Earlier co-pyrolysis work confirmed positive synergy between polyolefin and PET feedstocks, yet the study only focused on unmodified HZSM-5 without exploring bimetallic regulation of aromatic selectivity [12]. Similar synergistic effects have also been widely observed in co-pyrolysis systems of polycarbonate with polyolefins, where hydrogen transfer between different plastic components significantly promotes deoxygenation and aromatic formation [13,14]. Our research fills this gap by employing an Fe–Ni co-doping strategy.

Moreover, catalyst modification is the key to further optimize the selectivity of aromatic hydrocarbons. HZSM-5 is widely used in the preparation of aromatic hydrocarbons from plastic pyrolysis, owing to its unique pore structure and abundant acid sites. However, pristine HZSM-5 suffers from excessive acidity, severe coking and insufficient MAHs selectivity [15,16]. Modification with transition metals can regulate the acid distribution and pore structure of HZSM-5: Fe possesses high oxygen affinity, which can reduce total acidity and adjust the ratio of Brønsted acid to Lewis acid [17]; Ni can enhance hydrogenation capacity and promote deoxygenation reactions [18]. Furthermore, bimetallic modified catalysts usually exhibit superior catalytic performance compared with single-metal modified catalysts. For instance, Fe-Ni bimetallic loaded zeolite catalysts have been reported to significantly improve aromatic yield in catalytic pyrolysis due to the synergistic effect between dual metal sites [19,20].

Although existing studies have confirmed the effectiveness of co-pyrolysis synergism and metal modification [21,22], in-depth investigations on how Fe-Ni bimetals synergistically regulate the physicochemical properties of HZSM-5 and further affect the formation mechanism of MAHs during PET/LDPE co-pyrolysis are still insufficient. In this work, reaction parameters of co-pyrolysis were systematically optimized, and a series of HZSM-5 catalysts modified with different Fe/Ni mass ratios were fabricated. Combined with

characterization methods including XRD, BET, FTIR and NH_3-TPD, the structure-activity relationship between catalyst structure and catalytic performance was revealed, and the reaction pathways of MAHs production from PET/LDPE co-pyrolysis were elucidated. This study provides technical references and theoretical basis for the high-value utilization of waste plastics.

2. Results and Discussion

2.1. Catalyst Characterization Results

2.1.1. XRD Analysis

Prior to XRD detection, all pristine catalysts were ground to 80 mesh and dried overnight at 100 °C to eliminate adsorbed moisture, which could interfere with weak diffraction peaks of metal oxides. Figure 1 shows the XRD patterns of pristine HZSM-5 and metal-modified catalysts.

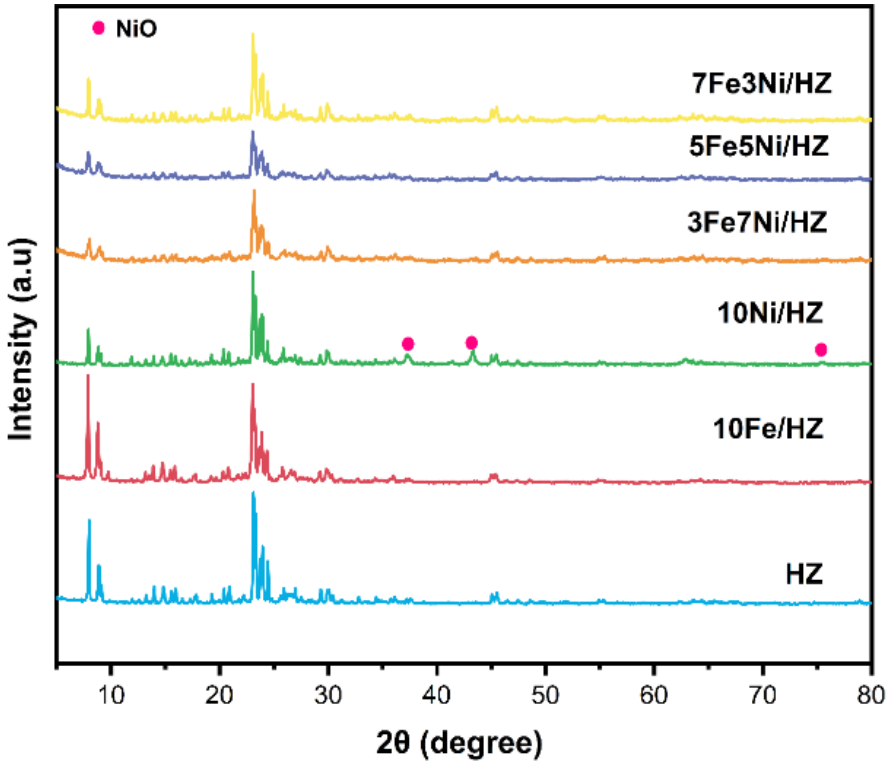


Figure 1. The XRD patterns of pristine HZSM-5 and metal-modified catalysts.

All pristine samples presented characteristic diffraction peaks of HZSM-5 at 2θ = 7.9°, 8.8°, 23.2°, 23.9° and 24.4°, indicating that metal loading did not destroy the topological crystal structure of HZSM-5 in the as-prepared catalysts [16]. No characteristic peaks of Fe or iron oxides were observed in the pattern of 10Fe/HZ, demonstrating that Fe species were highly dispersed on the carrier without forming large crystalline particles. Strong NiO diffraction signals were captured for monometallic 10Ni/HZ, indicating severe metal agglomeration after high-temperature calcination at 550 °C. We initially attempted lower calcination temperatures, yet incomplete precursor decomposition suppressed aromatic conversion efficiency. No characteristic peaks of Fe and Ni were detected for any bimetallic modified catalysts (3Fe7Ni/HZ, 5Fe5Ni/HZ, 7Fe3Ni/HZ), proving that the introduction of Fe effectively inhibited the agglomeration of NiO and promoted the uniform dispersion of bimetallic species on HZSM-5 [23]. In addition, the intensity of HZSM-5 characteristic

peaks of bimetallic catalysts decreased slightly, implying that the introduction of Fe and Ni caused a minor adverse effect on the crystallinity of the carrier.

2.1.2. BET Analysis

The pore structure parameters of different catalysts are listed in Table 1. The SBET, Vtotal and Dpore of pristine HZSM-5 were 396.27 m^2/g, 0.20 cm^3/g and 2.05 nm, respectively. The specific surface area of all metal-modified catalysts decreased, which was attributed to the deposition of metal particles on the carrier surface and inside pore channels, blocking partial pores [24]. 10Ni/HZ exhibited the lowest SBET (307.28 m^2/g) and Vtotal (0.17 cm^3/g), which was consistent with the NiO agglomeration phenomenon reflected by XRD results. The SBET of all bimetallic catalysts was higher than that of 10Ni/HZ, among which 7Fe3Ni/HZ possessed the maximum SBET (327.66 m^2/g), indicating that the synergistic dispersion of Fe and Ni helped retain more pore structures.

Table 1. The pore structure parameters of different catalysts.

Catalysts	SBET * (m^2/g)	Vtotal (cm^3/g)	Dpore size (nm)	Vmeso ** (cm^3/g)	Vmicro (cm^3/g)
HZ	396.27	0.20	2.05	0.08	0.12
10Fe/HZ	330.67	0.20	2.61	0.11	0.09
10Ni/HZ	307.28	0.17	2.15	0.07	0.10
3Fe7Ni/HZ	315.08	0.17	2.29	0.07	0.10
5Fe5Ni/HZ	320.85	0.19	2.47	0.09	0.10
7Fe3Ni/HZ	327.66	0.20	2.35	0.10	0.10

* SBET was calculated by BET method. ** Vmeso was estimated by t-plot method.

With the increase in Fe loading, the mesopore volume Vmeso of bimetallic catalysts gradually increased (0.07 cm^3/g for 3Fe7Ni/HZ and 0.10 cm^3/g for 7Fe3Ni/HZ). It suggested that the introduction of Fe might generate new mesopores based on original micropores. Larger mesopores facilitated the diffusion of reactant molecules to internal active sites of catalysts and promoted aromatization reactions [25]. However, excessively large pore channels would prolong the residence time of MAHs and induce condensation reactions to form PAHs and coke. The Dpore of 3Fe7Ni/HZ was 2.29 nm within the appropriate range, which guaranteed mass transfer efficiency and inhibited side reactions, laying a structural foundation for its excellent catalytic performance.

2.1.3. FTIR Analysis

Figure 2 presents the FTIR spectra of various catalysts. All samples showed characteristic absorption peaks of HZSM-5 near 570 cm^{-1}, 1100 cm^{-1}, 1635 cm^{-1}, 3450 cm^{-1} and 3620 cm^{-1}, further verifying that metal modification did not damage the skeleton structure of the carrier [26]. The absorption peak at 570 cm^{-1} corresponded to the vibration of five-membered rings of MFI topological structure; the peak at 1100 cm^{-1} was assigned to the asymmetric stretching vibration of T-O-T (T = Si/Al), which reflected the integrity of the zeolite skeleton; the peaks at 1635 cm^{-1} and 3450 cm^{-1} were attributed to the bending vibration and stretching vibration of surface hydroxyl groups (-OH); the peak at 3620 cm^{-1} belonged to the stretching vibration of hydroxyl groups on Al species.

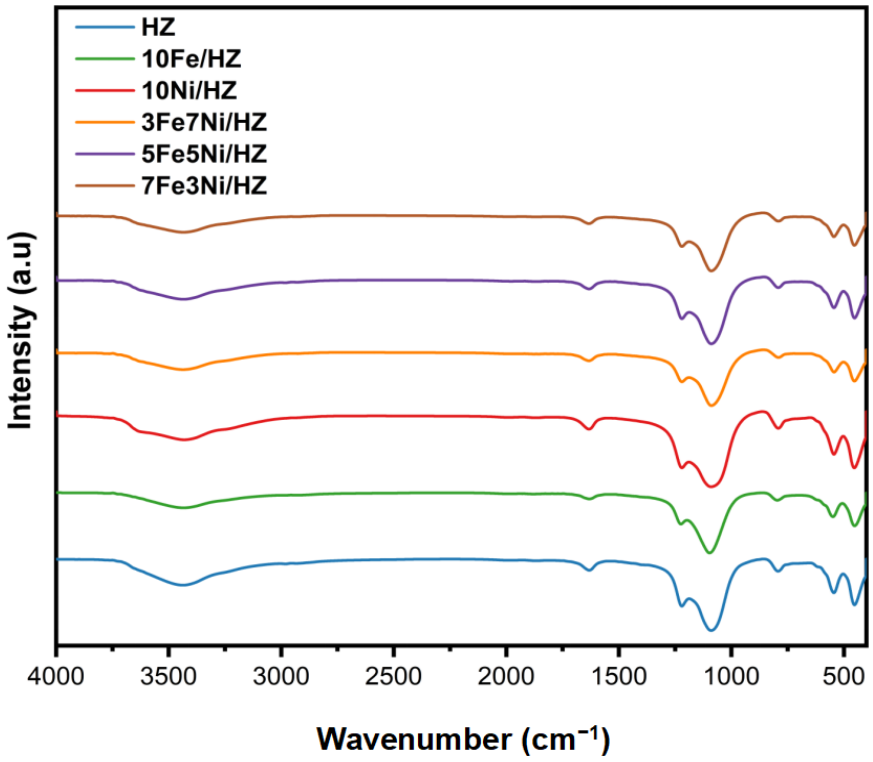


Figure 2. The FTIR spectra of various catalysts.

Compared with pristine HZSM-5, the absorption intensity of the Si-O framework band at 1100 cm^{-1} is markedly reduced for metal-modified catalysts. This phenomenon suggests that Fe and Ni species interact with surface hydroxyl groups of the support and attenuate the framework vibration of zeolite. No distinct characteristic peaks corresponding to metal oxides are detected for bimetallic samples, which is consistent with the high uniform dispersion of metallic species revealed by XRD patterns. Compared with pristine HZSM-5, the intensity of Si-O bond absorption peak at 1100 cm^{-1} of metal-modified catalysts decreased obviously, indicating that Fe and Ni interacted with surface hydroxyl groups of the carrier and weakened the skeleton vibration. No obvious characteristic peaks of metal oxides were observed for bimetallic catalysts, which was in accordance with the uniform metal dispersion results obtained from XRD tests.

2.1.4. NH_3-TPD Analysis

The acid properties of catalysts play a vital role in the reaction pathways of plastic pyrolysis. It should be noted that the NH_3-TPD tests in this work were conducted under identical experimental conditions for comparative analysis of relative acidity differences among samples, rather than absolute quantitative determination of acid content. In NH_3-TPD profiles, low-temperature peaks (120–300 °C) correspond to weak acid sites, and high-temperature peaks (300–500 °C) are assigned to strong acid sites. As shown in Figure 3, pristine HZSM-5 exhibited distinct weak acid peaks and strong acid peaks, suggesting abundant acid sites with a wide intensity distribution. For 10Fe/HZ, the strong acid peak disappeared completely, and the weak acid peak shifted to lower temperature with reduced intensity, indicating a significant decrease in relative total acidity. This was because Fe_2O_3 covered part of acid sites and regulated acid strength. For 10Ni/HZ, the intensity of weak acid peaks increased and shifted to higher temperature, and the strong acid peak was remarkably enhanced, which meant that Ni loading increased the relative strength of both weak and strong acid sites on the catalyst [18,27].

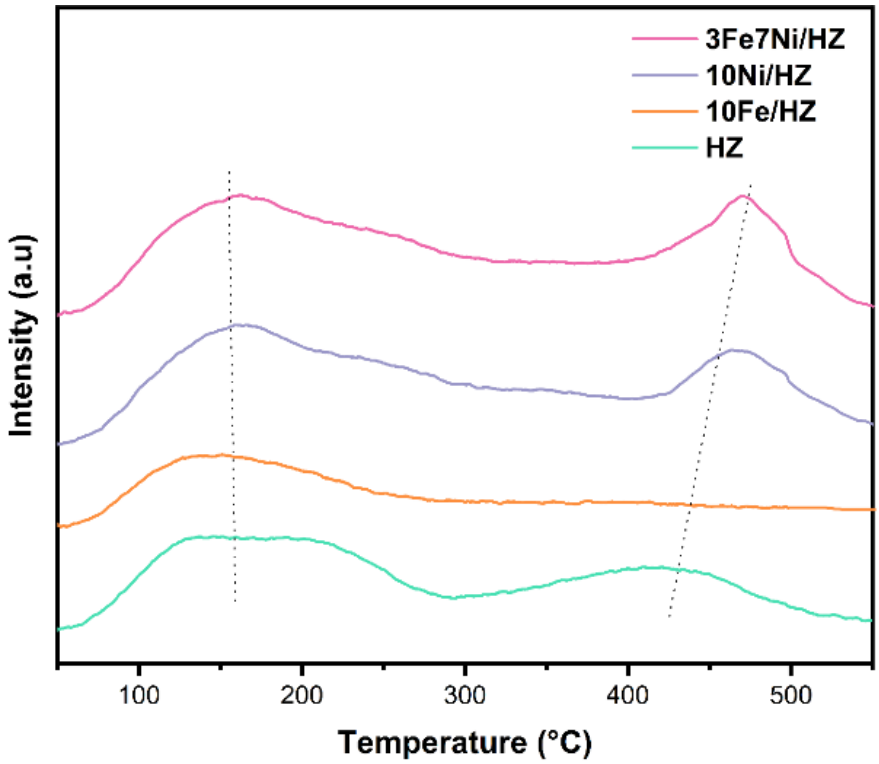


Figure 3. The NH_3-TPD profiles of various catalysts (The dashed lines represent the two desorption peaks in the low-temperature and high-temperature ranges.).

For bimetallic catalysts, the temperature of weak acid peaks was between that of 10Fe/HZ and 10Ni/HZ, and the strong acid peaks shifted to higher temperature with increased intensity. Among them, 3Fe7Ni/HZ possessed an appropriate intensity ratio of weak acid sites to strong acid sites. It retained sufficient strong acid sites to promote β-cracking of plastics, and the weak acid sites facilitated the alkylation reaction of benzene and toluene, providing favorable acid conditions for the improvement of MAHs selectivity [28].

2.2. Effects of Reaction Parameters on PET/LDPE Co-Pyrolysis

2.2.1. Effect of Pyrolysis Temperature on Products

Pyrolysis temperature is a key parameter for regulating product distribution. Figure 4 displays the variation in product yields during HZSM-5 catalyzed co-pyrolysis of PET/LDPE (1:9) within the temperature range of 500–650 °C (plastic-to-catalyst mass ratio = 2:1). The liquid yield increased first and then decreased with the rise in temperature: the liquid yield was 32.7 wt% at 500 °C, reached the maximum value of 38.0 wt% at 550 °C, and dropped to 35.4 wt% at 650 °C. The solid yield decreased sharply from 30.6 wt% (500 °C) to 17.4 wt% (550 °C) and increased slightly afterwards. Elevated temperature accelerated the cracking of plastics and converted high-boiling benzoic acid solid products into liquid and gaseous components. Nevertheless, when the temperature exceeded 550 °C, high temperature induced the condensation of MAHs to form PAHs and coke. When temperature exceeded 600 °C, obvious black coke deposits were observed on quartz tube inner walls, consistent with the rising PAHs fraction in GC–MS results. Meanwhile, the strong acidity of HZSM-5 accelerated carbon deposition of macromolecules and reduced catalyst activity, resulting in the decline of liquid yield [29]. Therefore, 550 °C was selected as the optimal pyrolysis temperature.

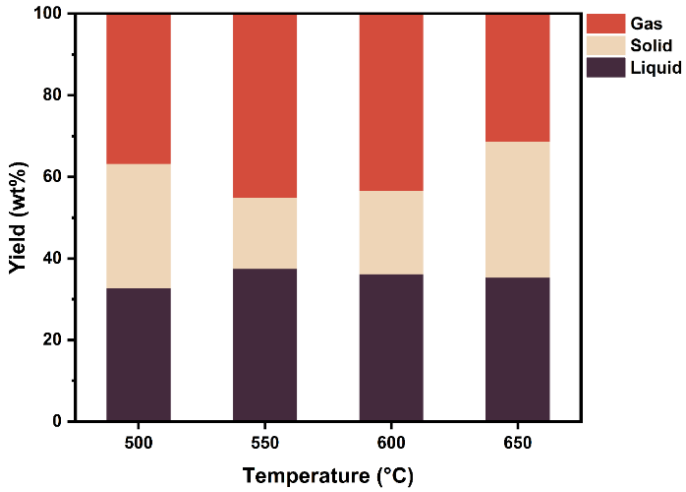


Figure 4. The variation in product yields during HZSM-5 catalyzed co-pyrolysis of PET/LDPE, Mass ratio: PET/LDPE = 1:9, Plastic/Catalyst = 2:1.

2.2.2. Effect of Plastic/Catalyst Mass Ratio on Products

Under the conditions of 550 °C and PET/LDPE mass ratio of 1:9, the influence of plastic/catalyst mass ratio (from 2:1 to 1:5) on products was investigated (Figure 5). As shown in Figure 5a, the liquid yield rose significantly from 37.5 wt% to 49.9 wt% with the increase in catalyst dosage and tended to be stable when the mass ratio reached 1:4. At plastic/catalyst ratio 1:2, white benzoic acid solid condensate completely disappeared, which we visually confirmed in ice-water condenser after each batch test. Increasing catalyst dosage enlarged the number of active sites in the reaction system, promoted ester hydrolysis and decarboxylation of benzoic acid derivatives, and improved the deoxygenation efficiency of oxygen-containing compounds.

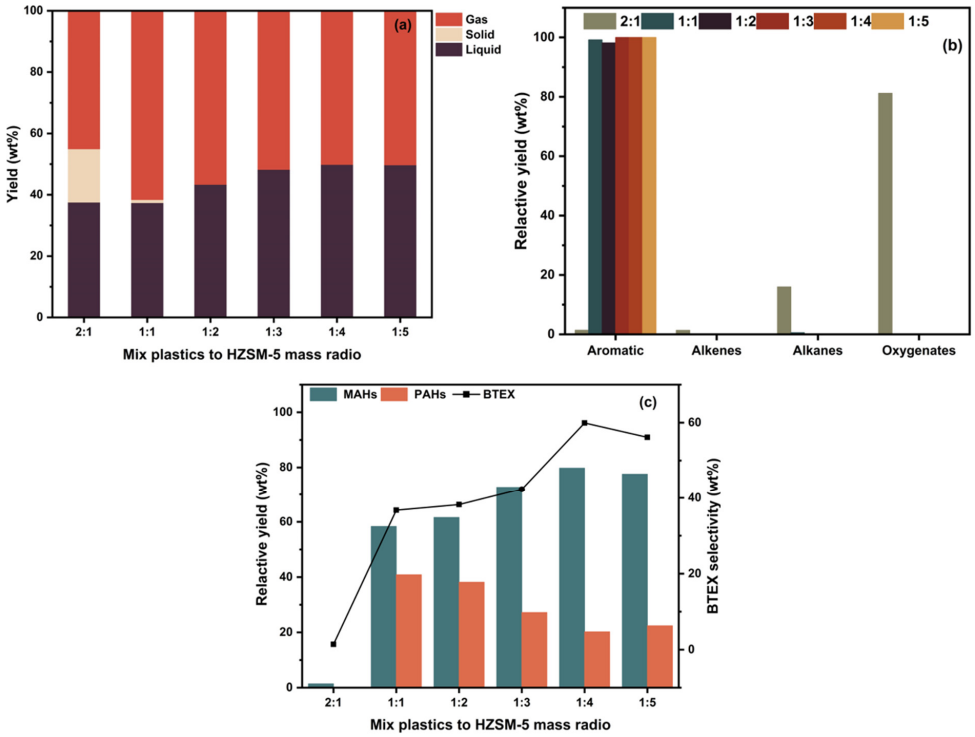


Figure 5. The effect of Plastic/Catalyst mass ratio on products at 550 °C and PET/LDPE mass ratio 1:9, (**a**) the variation in different product yields, (**b**) the selectivity of aromatic hydrocarbons, (**c**) the distribution of aromatic hydrocarbons.

Component analysis of liquid products (Figure 5b) showed that the selectivity of aromatic hydrocarbons increased from 1.4% to 100% with the addition of catalyst, while alkanes, olefins and oxygen-containing compounds gradually disappeared. This phenomenon was closely related to the radical reaction mechanism: the cleavage of PET ester bonds generated benzene radicals, and the breakage of C-C bonds in LDPE produced hydrogen radicals. Alkylation and hydrogen transfer reactions occurred on acid sites of catalysts to form aromatic hydrocarbons. Further analysis of aromatic hydrocarbon distribution (Figure 5c) revealed that the MAHs selectivity increased from 58.4% to 79.8% with the increase in catalyst dosage, but decreased to 77.6% at the mass ratio of 1:5. Excessive catalyst prolonged the residence time of benzene radicals in pore channels and promoted polymerization to form PAHs [30]. Thus, the optimal plastic-to-catalyst mass ratio was determined as 1:4.

2.2.3. Effect of PET/LDPE Mass Ratio on Products

With fixed temperature (550 °C) and plastic/catalyst mass ratio (1:4), the effect of PET/LDPE mass ratio on products was explored (Figure 6). As illustrated in Figure 6a, the liquid yield increased gradually with the rise in PET proportion and peaked at 80.2% when the PET/LDPE mass ratio was 2:3. The products turned into waxy solids if PET proportion continued to increase. Water was detected in liquid products starting from the PET/LDPE ratio of 3:7, and water content increased with the addition of PET. The increase in PET content raised the concentration of benzene radicals, promoted the hydrogenation of benzoic acid to form benzenediol, and further dehydrated to generate benzaldehyde and water [31]. When the dosage of PET exceeded that of LDPE, the catalytic sites of HZSM-5 were insufficient to complete the deoxygenation of all PET. Excess PET was directly cracked to produce terephthalic acid and other solid products, leading to a sharp drop in liquid yield.

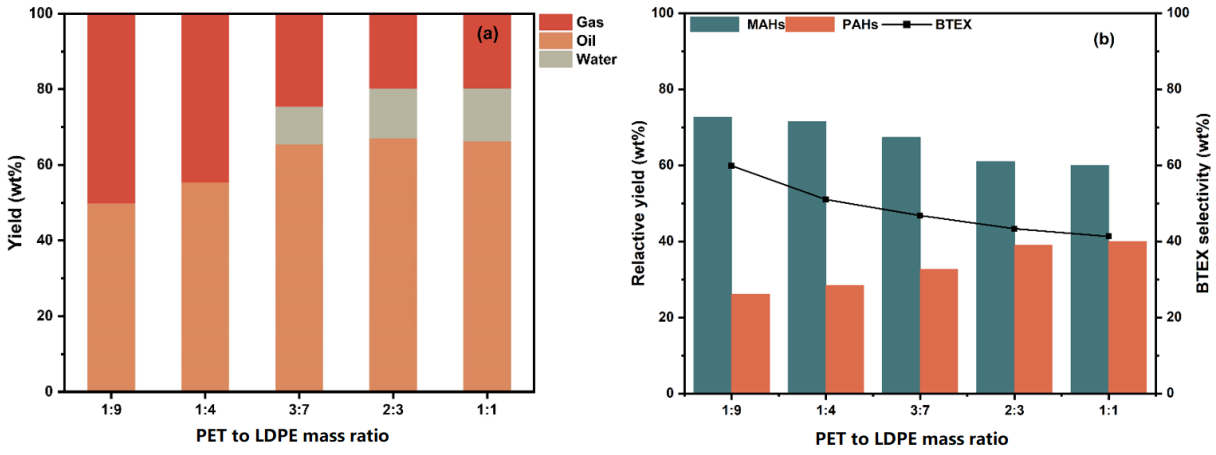


Figure 6. The effect of PET/LDPE mass ratio at 550 °C and Plastic/Catalyst = 1:4, (**a**) the variation in different product yields, (**b**) the distribution of aromatic hydrocarbons.

According to the distribution of aromatic hydrocarbons (Figure 6b), the MAHs selectivity decreased from 72.8% to 60.0% and BTEX selectivity dropped from 59.9% to 41.3% with the increase in PET proportion. Higher PET content produced more benzene radicals and accelerated the condensation and over-alkylation of benzene rings, resulting in the increase in PAHs content. Meanwhile, the reduction in LDPE proportion decreased olefins and hydrogen sources in the system, which inhibited the generation of BTEX [10]. Considering both liquid yield and MAHs selectivity, the optimal PET/LDPE mass ratio was confirmed as 2:3.

2.3. Effect of Bimetallic Modification on Aromatic Hydrocarbon Components

The catalytic performance of different catalysts was evaluated under the optimal reaction conditions (550 °C, Plastic/Catalyst mass ratio = 1:4, PET/LDPE mass ratio = 2:3) (Figure 7). Compared with pristine HZ, the total aromatic hydrocarbon content of 10Ni/HZ decreased to 90.7 wt%, while the MAHs selectivity increased to 67.1 wt%. Ni enhanced hydrogenation capacity and facilitated deoxygenation, but the agglomeration of NiO likely increased catalyst coking and thus reduced overall catalytic activity. The proportion of detectable aromatic hydrocarbons in the liquid products over 10Fe/HZ was 100%, and the MAHs selectivity reached 69.7 wt%. Fe regulated the acid distribution and the ratio of Brønsted acid to Lewis acid, which promoted the alkylation of benzene radicals [17].

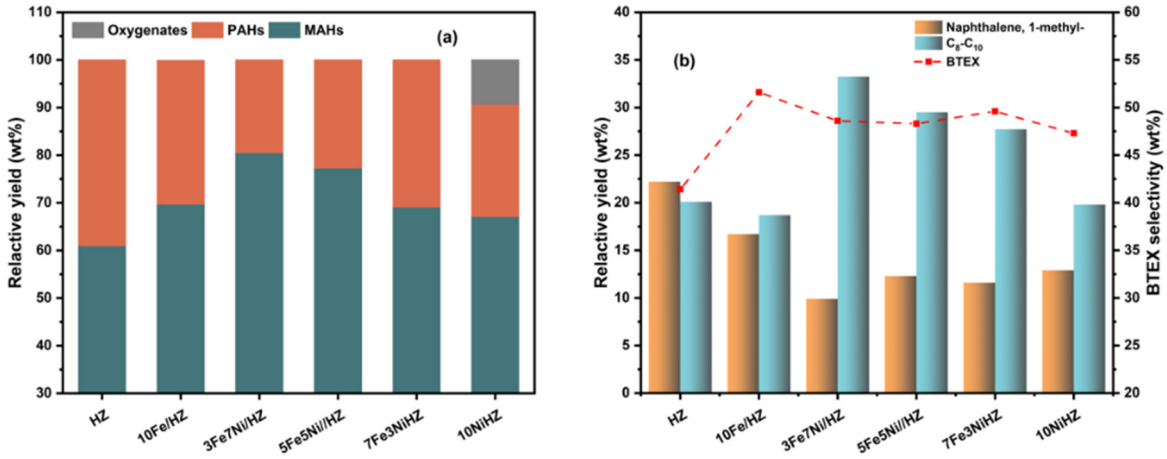


Figure 7. The effect of bimetallic modification on aromatic hydrocarbon components at 550 °C, Plastic/Catalyst = 1:4 and PET/LDPE = 2:3, (**a**) the components of aromatic hydrocarbons, (**b**) the distribution of aromatic hydrocarbons.

All bimetallic catalysts exhibited higher MAHs selectivity than single-metal modified catalysts and pristine HZSM-5, which was consistent with the synergistic catalytic advantage of dual metal zeolite catalysts reported in the previous literature [19]. Among them, 3Fe7Ni/HZ achieved the optimal performance with the MAHs selectivity of 80.5%, which was about 20% higher than that of pristine HZ. Further analysis of aromatic hydrocarbon components (Figure 7b) showed that bimetallic modification had little influence on BTEX selectivity. The improvement of MAHs selectivity was mainly attributed to the increase in C_8–C_{10} alkylbenzene content. The selectivity of C_8–C_{10} alkylbenzene over 3Fe7Ni/HZ was as high as 33.2wt%, while the selectivity of methylnaphthalene (main component of PAHs) decreased to 9.9wt%. The selectivity of C_8–C_{10} alkylbenzene declined gradually with the increase in Fe loading, and excessive Fe inhibited the formation of MAHs. It was obvious that the Fe/Ni ratio played a decisive role in catalytic performance [32]. The 3Fe7Ni/HZ catalyst balanced the acidity and pore structure, promoted alkylation reactions and suppressed the generation of PAHs, so as to maximize the selectivity of MAHs.

2.4. Reaction Pathways of PET/LDPE Co-Pyrolysis

It should be noted that the proposed reaction pathways are mainly based on liquid product analysis, while gas composition was not further characterized in this study.

Based on experimental results and characterization analysis, the reaction pathways of PET/LDPE co-pyrolysis over 3Fe7Ni/HZ were proposed (Figure 8). MAHs were mainly generated via three routes:

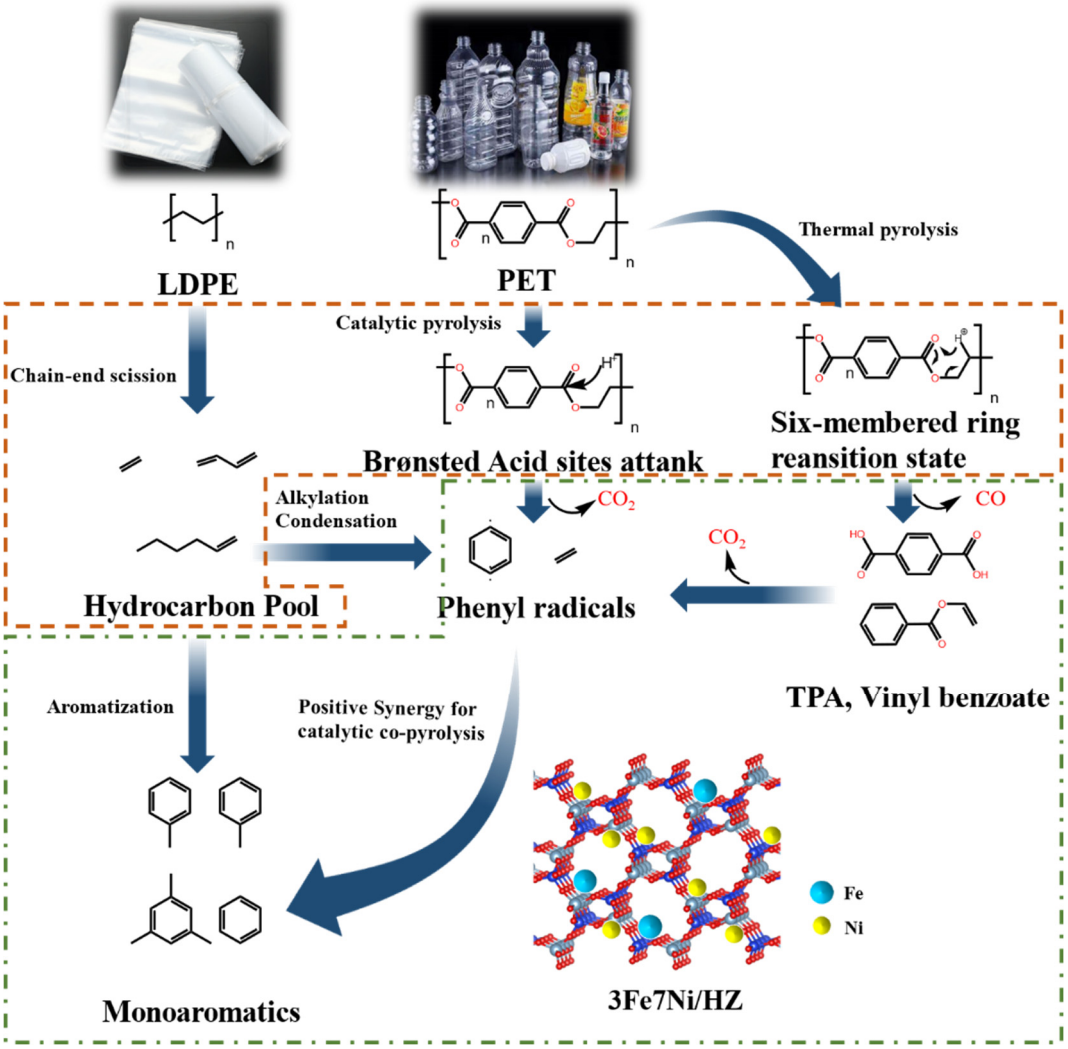


Figure 8. The reaction pathways of PET/LDPE co-pyrolysis. The red dashed box and the green box indicate pyrolysis and radical-intermediate formation, catalytic aromatization over Fe-Ni/HZSM-5, respectively.

Cracking and deoxygenation of PET: PET underwent non-catalytic pyrolysis via six-membered ring transition state to form intermediates such as benzoic acid and terephthalic acid. Decarboxylation and decarbonylation reactions occurred on acid sites of catalysts to produce benzene radicals and short-chain olefins, which further formed aromatic hydrocarbons via alkylation. Meanwhile, protonic acid on catalysts attacked C-C and C-O bonds of PET, and terminal oxygen was removed during deoxygenation process [33].

Aromatization of LDPE: LDPE produced long-chain olefins through random cracking or chain cracking, which were dehydrogenated and cyclized on strong acid sites of catalysts to form aromatic hydrocarbons [34].

Synergistic reaction: Hydrogen radicals generated from LDPE pyrolysis acted as hydrogen sources for benzene radicals derived from PET, inhibiting the polymerization of benzene radicals and promoting alkylation reactions to form MAHs. In addition, carbon cations produced by LDPE reacted with benzene radicals and further increased the yield of MAHs [25].

The synergistic effect of Fe and Ni on 3Fe7Ni/HZ was the key to the improvement of MAHs selectivity. Fe restrained the agglomeration of NiO, improved metal dispersion and reduced catalyst coking. It should be noted that no dedicated coke characterization was

performed in this work. The discussion of carbon deposition was based on indirect experimental evidence and literature reports, rather than direct quantitative measurements [23]. Bimetallic loading balanced the catalyst acidity, strengthened cracking capacity and accelerated the alkylation of benzene radicals. The appropriate pore structure guaranteed the mass transfer efficiency of reactant molecules and prevented the condensation of MAHs into PAHs [35], finally realizing the efficient and targeted preparation of MAHs. For our follow-up research focusing on in-depth acid catalytic mechanism, pyridine-FTIR measurements will be implemented to separately quantify Brønsted and Lewis acid sites. This characterization can supply direct evidence to elaborate how Fe-Ni bimetals regulate two types of acid sites and further affect aromatic formation pathways.

3. Materials and Methods

3.1. Raw Materials

PET (150 mesh) was purchased from Fengtai Polymer Materials Co., Ltd. (Beijing, China); LDPE (100 mesh) was supplied by Dongguan Xingwang Plastic Raw Materials Co., Ltd (Dongguan, China). Ferric nitrate nonahydrate ($Fe(NO_3)_3 \cdot 9H_2O$, analytical grade) and nickel nitrate hexahydrate ($Ni(NO_3)_2 \cdot 6H_2O$, analytical grade) were obtained from Shanghai Aladdin Biochemical Technology Co., Ltd (Shanghai, China). HZSM-5 zeolite (Si/Al = 25) was purchased from Nankai University Catalyst Factory (Tianjin, China). All raw materials were dried at 80 °C for 12 h before use. HZSM-5 zeolite was calcined in a muffle furnace at 550 °C for 4 h to remove adsorbed impurities, and then cooled and stored in a desiccator for later use.

After pyrolysis finished, dichloromethane solvent was used to rinse condensation pipelines three times to fully recover heavy aromatic fractions, and extract liquids were stored at −20 °C to avoid volatile BTEX loss before GC–MS analysis. Pd/trap-HZSM-5 based studies have shown that low-temperature storage is essential to preserve light aromatic components in pyrolysis oil [36].

3.2. Catalyst Preparation

Fe-Ni bimetallic modified HZSM-5 catalysts were prepared by the incipient wetness impregnation method with a total metal loading of 10 wt%, which is the most common preparation method for metal-modified zeolite catalysts in plastic catalytic pyrolysis research [24,35]. The detailed procedures are as follows:

(1) Ferric nitrate nonahydrate and nickel nitrate hexahydrate were weighed accurately according to Fe/Ni mass ratios (10:0, 3:7, 5:5, 7:3, 0:10) and dissolved in 4 mL of deionized water. The mixture was magnetically stirred until complete dissolution.
(2) A total of 4 g of pre-treated HZSM-5 zeolite was added into the above solution, and the mixture was continuously stirred for 4 h to ensure uniform impregnation of metal precursors on the carrier surface. We first tried 6 h impregnation, but 4 h stirring achieved uniform metal loading without excessive precursor waste, hence it was adopted in all catalyst synthesis batches.
(3) The mixture was dried in an oven at 80 °C for 12 h, followed by calcination in a muffle furnace at 550 °C for 4 h. After natural cooling, the solid was ground and sieved through an 80-mesh sieve. The obtained catalysts were denoted as 10Fe/HZ, 3Fe7Ni/HZ, 5Fe5Ni/HZ, 7Fe3Ni/HZ and 10Ni/HZ, respectively, and the pristine HZSM-5 was marked as HZ.

3.3. Experimental Apparatus and Procedures

Catalytic co-pyrolysis experiments were carried out in a fast pyrolysis reactor, as shown in Figure 9. The apparatus was composed of a nitrogen cylinder, pressure reducing valve,

flow meter, quartz tube reactor (inner diameter: 16 mm, length: 500 mm), condensation system (ice water bath at 0 °C), and gas collection bags.

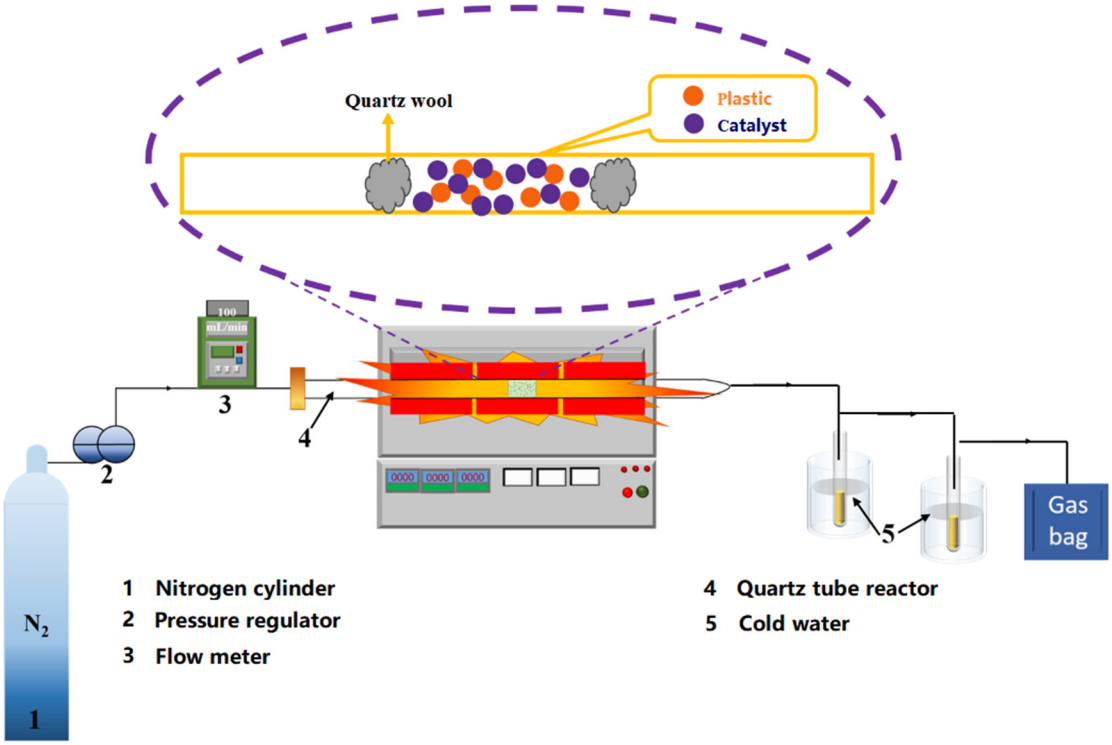


Figure 9. Schematic diagram of the reaction device.

The specific experimental processes are listed below:

(1) Raw plastic mixtures and catalysts with preset ratios were mixed thoroughly, with a total mass of 0.8 g. The mixture was loaded into the middle of the quartz tube and fixed with quartz wool at both ends.

(2) The experimental apparatus was connected. High-purity nitrogen was purged at a flow rate of 100 mL/min for 30 min to remove air inside the system. Meanwhile, the gas outlet end of the quartz tube was preheated to 300 °C to prevent premature condensation of volatile components.

(3) The quartz tube was heated to the set temperature at a heating rate of 25 °C/s and kept at a constant temperature for 10 min. Pyrolysis volatiles were condensed and collected in the condenser, and non-condensable gas was stored in gas collection bags.

(4) After the experiment, chromatographically pure dichloromethane was used to rinse the inner wall of the condenser and quartz tube. The rinsing solution was mixed with condensed liquid and stored in a refrigerator at -20 °C for subsequent analysis.

(5) All experiments were repeated three times, and the average values were adopted to guarantee data reliability.

3.4. Product Analysis

3.4.1. Calculation of Product Yield

Pyrolysis products were divided into solid, liquid and gas phases. Product yields were calculated based on the law of mass conservation.

Solid yield (Y_{solid}): The ratio of the mass of residual solid in the quartz tube (excluding catalyst and quartz wool) to the total mass of plastic raw materials.

Liquid yield (Y_{liquid}): The ratio of the net mass of condensed liquid to the total mass of plastic raw materials.

Gas yield (Y_{gas}): Calculated by subtracting solid yield and liquid yield from 100%.

$$Y_{solid} = \frac{M_{solid\ residue} - M_{catalyst} - M_{quartz\ wool}}{M_{plastic}} \times 100\% \quad (1)$$

$$Y_{liquid} = \frac{M_{condenser+liquid} - M_{condenser}}{M_{plastic}} \times 100\% \quad (2)$$

$$Y_{gas} = 100\% - Y_{solid} - Y_{liquid} \quad (3)$$

where $M_{solid\ residue}$ = total mass of residual solid in quartz tube (g); $M_{catalyst}$ = total mass of catalyst (g); $M_{quartz\ wool}$ = mass of quartz wool (g); $M_{plastic}$ = total mass of plastic raw materials (g); and $M_{condenser}$ and $M_{condenser+liquid}$ represent the mass of empty condenser and condenser with liquid after pyrolysis (g), respectively.

3.4.2. Component Analysis of Liquid Products

The components of liquid products were qualitatively and quantitatively analyzed by Shimadzu QP 2010 Ultra (Shimadzu Corporation, Kyoto, Japan) gas chromatography-mass spectrometry (GC–MS). After extraction with dichloromethane, 1 μL of sample was injected for analysis. The analytical conditions are as follows:

Chromatographic column: DB-WAXetr (30.0 m × 0.25 mm × 0.25 μm);

Carrier gas: high-purity He, flow rate: 1.0 mL/min, split ratio: 1:1;

Column temperature program: maintained at 50 °C for 3 min, raised to 200 °C at 4 °C/min, then increased to 280 °C at 40 °C/min and held for 5 min.

Mass spectrometry conditions: Interface temperature: 250 °C; solvent delay: 1.8 min; scanning range: 33–600 amu; and scanning rate: 2000 amu/s.

Qualitative analysis was performed by matching with the NIST11 mass spectral library, and quantitative analysis adopted the peak area normalization method [37].

3.5. Catalyst Characterization

X-ray Diffraction (XRD): Tests were conducted on an XPert PRO diffractometer (Malvern Panalytical, Almelo, The Netherlands) with Cu Kα radiation (λ = 1.541862 nm). The tube voltage was 40 kV, tube current was 100 mA, the step size was 0.02°, the scanning rate was 10°/min, and the 2θ scanning range was 5.0–80.0°. The crystal structure and metal dispersion of the catalysts were analyzed.

Brunauer–Emmett–Teller (BET) Analysis: A Micromeritics ASAP 2460 analyzer (Micromeritics Instrument Corporation, Norcross, GA, USA) was used for nitrogen adsorption–desorption tests at −196 °C. Samples were degassed at 300 °C for 8 h in advance. The specific surface area (SBET) was calculated by the BET method; pore diameter (Dpore) and total pore volume (Vtotal) were calculated via the BJH model; micropore volume (Vmicro) and mesopore volume (Vmeso) were estimated by the t-plot method.

Fourier Transform Infrared Spectroscopy (FTIR): A Nicolet 5700 spectrometer (Thermo Fisher Scientific, Madison, WI, USA) was applied with a resolution of 4 cm^{-1} and a scan number of 32 times in the wavenumber range of 4000–400 cm^{-1}, to analyze functional groups and skeleton structure of catalysts [38].

NH_3-Temperature Programmed Desorption (NH_3-TPD): Measurements were carried out on a GC7890T analyzer (Shimadzu Corporation, Kyoto, Japan). Furthermore, 0.3 g of sample was pre-treated in He flow at 350 °C for 60 min and then cooled to 50 °C for NH_3 adsorption (1% NH_3-He mixed gas). Subsequently, the temperature was raised to 500 °C at a rate of 10 °C/min, and desorbed NH_3 was detected by a TCD detector to analyze the strength and quantity of acid sites on catalysts.

4. Conclusions

In this study, the co-pyrolysis reaction parameters of PET/LDPE and Fe-Ni bimetallic modified HZSM-5 catalysts were optimized to realize the directional conversion of oxygen-containing waste plastics into high-selectivity monocyclic aromatic hydrocarbons.

The main conclusions are as follows:

(1) The optimal co-pyrolysis reaction parameters were determined: pyrolysis temperature of 550 °C, plastic-to-catalyst mass ratio of 1:4 and PET/LDPE mass ratio of 2:3. Under these conditions, the liquid yield reached 80.2%, all detectable compounds in pyrolysis oil were aromatic hydrocarbons, and the MAHs selectivity was 79.8%. LDPE provided hydrogen sources for the cracking of PET, and the synergistic effect between the two plastics promoted deoxygenation and significantly improved product quality.

(2) Fe-Ni bimetallic modification remarkably enhanced the catalytic performance of HZSM-5. The 3Fe7Ni/HZ catalyst showed the best catalytic activity with the MAHs selectivity of 80.5%, an increase of about 20% compared with pristine HZSM-5. Bimetallic loading realized uniform metal dispersion on the carrier and helped reduce carbon deposition tendency. Meanwhile, the acidity of the catalyst was balanced, which promoted the alkylation of benzene radicals and inhibited the polymerization of MAHs into PAHs.

(3) Reaction pathway analysis indicated that MAHs were formed through three processes: cracking and deoxygenation of PET, aromatization of LDPE and synergistic reactions between the two plastics. The combined effect of pore structure and acid distribution of 3Fe7Ni/HZ created favorable conditions for mass transfer and catalytic reactions, achieving efficient directional production of MAHs.

This research provides a novel technical scheme for the high-value utilization of waste plastics. Further studies can focus on exploring the co-pyrolysis effect of other hydrogen-rich raw materials and oxygen-containing plastics and optimizing catalyst preparation processes to lay a foundation for industrial application.

Author Contributions: Writing—original draft, formal analysis, data curation, H.Y.; Writing—reviewed editing, resources, validation, C.Z.; Data curation, L.S.; Investigation, H.F. and N.X. All authors have read and agreed to the published version of the manuscript.

Funding: This research was supported by Key Science and Technology Project of Henan Province (No. 262102220089), Key Research Projects of Higher Education Institutions in Henan Province (No. 25B610011), Zhengzhou Basic and Applied Basic Research Project (No. ZZSZX202432).

Data Availability Statement: Data are contained within the article and will be made available upon request.

Conflicts of Interest: The authors declare no conflicts of interest.

References

1. Geyer, R.; Jambeck, J.R.; Law, K.L. Production, use, and fate of all plastics ever made. *Sci. Adv.* **2017**, *3*, e1700782. [CrossRef] [PubMed]
2. Mishra, R.; Kumar, A.; Singh, E.; Kumar, S. Recent Research Advancements in Catalytic Pyrolysis of Plastic Waste. *ACS Sustain. Chem. Eng.* **2023**, *11*, 2033–2049. [CrossRef]
3. Anuar Sharuddin, S.D.; Abnisa, F.; Wan Daud, W.M.A.; Aroua, M.K. A review on pyrolysis of plastic wastes. *Energy Convers. Manag.* **2016**, *115*, 308–326. [CrossRef]
4. Peng, Y.; Wang, Y.; Ke, L.; Dai, L.; Wu, Q.; Cobb, K.; Zeng, Y.; Zou, R.; Liu, Y.; Ruan, R. A review on catalytic pyrolysis of plastic wastes to high-value products. *Energy Convers. Manag.* **2022**, *254*, 115243. [CrossRef]
5. Zhang, F.; Zeng, M.; Yappert, R.D.; Sun, J.; Lee, Y.-H.; Lapointe, A.M.; Peters, B.; Abu-Omar, M.M.; Scott, S.L. Polyethylene upcycling to long-chain alkylaromatics by tandem hydrogenolysis aromatization. *Science* **2020**, *370*, 437–441. [CrossRef] [PubMed]

6. Shao, Y.; Kong, L.; Fan, M.; Sun, K.; Gao, G.; Li, C.; Zhang, L.; Zhang, S.; Wang, Y.; Hu, X. Synergy between Cu and Lewis Acidic Sites in Cu/Zn-FeOx Catalysts for the Selective Conversion of Poly (ethylene terephthalate) Waste to p-Xylene and Ethylene Glycol. *ACS Sustain. Chem. Eng.* **2024**, *12*, 3818–3830. [CrossRef]
7. Dhahak, A.; Hild, G.; Rouaud, M.; Mauviel, G.; Burkle-Vitzthum, V. Slow pyrolysis of polyethylene terephthalate: Online monitoring of gas production and quantitative analysis of waxy products. *J. Anal. Appl. Pyrolysis* **2019**, *142*, 104664. [CrossRef]
8. Kumagai, S.; Yamasaki, R.; Kameda, T.; Saito, Y.; Watanabe, A.; Watanabe, C.; Teramae, N.; Yoshioka, T. Tandem μ-reactor-GC/MS for online monitoring of aromatic hydrocarbon production via CaO-catalysed PET pyrolysis. *React. Chem. Eng.* **2017**, *2*, 776–784. [CrossRef]
9. Lu, S.; Jing, Y.; Feng, B.; Guo, Y.; Liu, X.; Wang, Y. H_2-free Plastic Conversion: Converting PET back to BTX by Unlocking Hidden Hydrogen. *Chem. Sus. Chem.* **2021**, *14*, 4242–4250. [CrossRef] [PubMed]
10. Xue, X.; Mi, J.; Huang, F.; Wang, J.; Chen, L.; Liang, J. Aromatics production from segmented co-pyrolysis of poplar sawdust and high-density polyethylene: Enhancing the synergistic effects. *J. Anal. Appl. Pyrolysis* **2023**, *170*, 105909. [CrossRef]
11. Jin, X.; Lee, J.H.; Choi, J.W. Catalytic co-pyrolysis of woody biomass with waste plastics: Effects of HZSM-5 and pyrolysis temperature on producing high-value pyrolytic products and reducing wax formation. *Energy* **2022**, *239*, 121739. [CrossRef]
12. Okonsky, S.T.; Krishna, J.V.J.; Toraman, H.E. Catalytic co-pyrolysis of LDPE and PET with HZSM-5, H-beta, and HY: Experiments and kinetic modelling. *React. Chem. Eng.* **2022**, *7*, 2175–2191. [CrossRef]
13. Sun, K.; Wang, W.; Themelis, N.J.; Bourtsalas, A.C.T.; Huang, Q. Catalytic co-pyrolysis of polycarbonate and polyethylene/polypropylene mixtures: Promotion of oil deoxygenation and aromatic hydrocarbon formation. *Fuel* **2021**, *285*, 119143. [CrossRef]
14. Liu, X.; Burra, K.R.G.; Wang, Z.; Li, J.; Che, D.; Gupta, A.K. Towards enhanced understanding of synergistic effects in co-pyrolysis of pinewood and polycarbonate. *Appl. Energy* **2021**, *289*, 116662. [CrossRef]
15. Dong, Z.; Chen, W.; Xu, K.; Liu, Y.; Wu, J.; Zhang, F. Understanding the Structure–Activity Relationships in Catalytic Conversion of Polyolefin Plastics by Zeolite-Based Catalysts: A Critical Review. *ACS Catal.* **2022**, *12*, 14882–14901. [CrossRef]
16. Inayat, A.; Inayat, A.; Schwieger, W.; Sokolova, B.; Lestinsky, P. Enhancing aromatics and olefins yields in thermo-catalytic pyrolysis of LDPE over zeolites: Role of staged catalysis and acid site density of HZSM-5. *Fuel* **2022**, *314*, 123071. [CrossRef]
17. He, Y.; Chen, J.; Mo, Z.; Hu, C.; Li, D.; Tu, J.; Lin, C.; Wang, Y.; Liu, D.; Wang, T. Controlling Diels-Alder reactions in catalytic pyrolysis of sawdust and polypropylene by coupling CO_2 atmosphere and Fe-modified zeolite for enhanced light aromatics production. *J. Hazard. Mater.* **2023**, *455*, 131547. [CrossRef] [PubMed]
18. Pan, Z.; Xue, X.; Zhang, C.; Wang, D.; Xie, Y.; Zhang, R. Production of aromatic hydrocarbons by hydro-liquefaction of high-density polyethylene (HDPE) over Ni/HZSM-5. *J. Anal. Appl. Pyrolysis* **2018**, *136*, 208–214. [CrossRef]
19. Li, Y.; Yellezuome, D.; Cai, J.; Tao, S.; Liu, R. Insight into the synergistic performance during ex-situ catalytic co-pyrolysis of poplar sawdust and polypropylene over Fe-Ni/ZSM-5 for the enhancement of aromatics. *Ind. Crop. Prod.* **2023**, *193*, 116249. [CrossRef]
20. Li, C.; Nishu; Yellezuome, D.; Li, Y.; Liu, R.; Cai, J. Enhancing bio-aromatics yield in bio-oil from catalytic fast pyrolysis of bamboo residues over bi-metallic catalyst and reaction mechanism based on quantum computing. *Fuel* **2023**, *336*, 127158. [CrossRef]
21. Zheng, K.; Wu, Y.; Hu, Z.; Wang, S.; Jiao, X.; Zhu, J.; Sun, Y.; Xie, Y. Progress and perspective for conversion of plastic wastes into valuable chemicals. *Chem. Soc. Rev.* **2022**, *51*, 8553–8574. [CrossRef] [PubMed]
22. Lee, K.; Jing, Y.; Wang, Y.; Yan, N. A unified view on catalytic conversion of biomass and waste plastics. *Nat. Rev. Chem.* **2022**, *6*, 635–652. [CrossRef] [PubMed]
23. Yao, D.; Wu, C.; Yang, H.; Zhang, Y.; Nahil, M.A.; Chen, Y.; Williams, P.T.; Chen, H. Co-production of hydrogen and carbon nanotubes from catalytic pyrolysis of waste plastics on Ni-Fe bimetallic catalyst. *Energy Convers. Manag.* **2017**, *148*, 692–700. [CrossRef]
24. Qian, K.; Tian, W.; Yin, L.; Yang, Z.; Tian, F.; Chen, D. Aromatic production from high-density polyethylene over zinc promoted HZSM-5. *Appl. Catal. B Environ. Energy* **2023**, *339*, 123159. [CrossRef]
25. Wang, J.; Jiang, J.; Sun, Y.; Meng, X.; Wang, X.; Ruan, R.; Ragauskas, A.J.; Tsang, D.C.W. Heterogeneous Diels-Alder tandem catalysis for converting cellulose and polyethylene into BTX. *J. Hazard. Mater.* **2021**, *414*, 125418. [CrossRef] [PubMed]
26. Zhu, L.; Huang, M.; Ma, Z.; Cai, B.; Zhang, W.; Peng, H.; Chen, D. Valorisation of waste biomass and plastics toward light aromatics: Co-catalytic fast pyrolysis of torrefied bamboo and polyethylene over alkali and acid treated hierarchical HZSM-5. *Fuel* **2023**, *349*, 128734. [CrossRef]
27. Qian, K.; Tian, W.; Li, W.; Wu, S.; Chen, D.; Feng, Y. Catalytic Pyrolysis of Waste Plastics over Industrial Organic Solid-Waste-Derived Activated Carbon: Impacts of Activation Agents. *Processes* **2022**, *10*, 2668. [CrossRef]
28. Zhang, L.-Y.; Cao, J.-P.; Ren, X.-Y.; Feng, X.-B.; Wang, J.-X.; He, Z.-M.; Liu, T.-L.; Yang, Z.; Zhao, X.-Y.; Bai, H.-C. Catalytic Upgrading of Cellulose Pyrolysis Volatiles over Ce Modified Hierarchical ZSM-5 Zeolite: Insight into the Effect of Acid Properties on Light Aromatics and Catalyst Stability. *Ind. Eng. Chem. Res.* **2022**, *61*, 287–298. [CrossRef]
29. Xue, Y.; Johnston, P.; Bai, X. Effect of catalyst contact mode and gas atmosphere during catalytic pyrolysis of waste plastics. *Energy Convers. Manag.* **2017**, *142*, 441–451. [CrossRef]

30. Zhang, J.; Ma, M.; Chen, Z.; Zhang, X.; Yang, H.; Wang, X.; Feng, H.; Yu, J.; Gao, S. Production of monocyclic aromatics and light olefins through ex-situ catalytic pyrolysis of low-density polyethylene over Ga/P/ZSM-5 catalyst. *J. Energy Inst.* **2023**, *108*, 101235. [CrossRef]
31. Yoshioka, T.; Handa, T.; Grause, G.; Lei, Z.; Inomata, H.; Mizoguchi, T. Effects of metal oxides on the pyrolysis of poly(ethylene terephthalate). *J. Anal. Appl. Pyrolysis* **2005**, *73*, 139–144. [CrossRef]
32. Zheng, X.; Zhong, Z.; Zhang, B.; Du, H.; Wang, W.; Li, Q.; Yang, Y.; Qi, R.; Ye, Q.; Li, Z. Preparation of monocyclic aromatic hydrocarbons from industrial lignin residue and polyethylene co-pyrolysis by microwave-assisted in fluidized bed based on bimetal-loaded HZSM-5/MCM-41 core-shell catalyst. *Fuel* **2024**, *364*, 131100. [CrossRef]
33. Jing, Y.; Shakouri, M.; Liu, X.; Hu, Y.; Guo, Y.; Wang, Y. Breaking C–C Bonds and Preserving C–O Bonds in Aromatic Plastics and Lignin via a Reversing Bond Energy Cleavage Strategy. *ACS Catal.* **2022**, *12*, 10690–10699. [CrossRef]
34. Wang, W.; Yao, C.; Ge, X.; Pu, X.; Yuan, J.; Sun, W.; Chen, W.; Feng, X.; Qian, G.; Duan, X.; et al. Catalytic conversion of polyethylene into aromatics with Pt/ZSM-5: Insights into reaction pathways and rate-controlling step regulation. *J. Mater. Chem. A* **2023**, *11*, 14933–14940. [CrossRef]
35. Kim, S.; Park, C.; Lee, J. Reduction of polycyclic compounds and biphenyls generated by pyrolysis of industrial plastic waste by using supported metal catalysts: A case study of polyethylene terephthalate treatment. *J. Hazard. Mater.* **2020**, *392*, 122464. [CrossRef] [PubMed]
36. Chen, W.; Xu, X.; Zhang, C.; Feng, Y.; Wang, Y.; Wang, J.; Zhang, R. A novel production of monocyclic aromatic hydrocarbons via one-step catalytic conversion of pine sawdust and waste plastics over Pd/trap-HZSM-5. *Fuel* **2021**, *293*, 120503. [CrossRef]
37. Li, K.; Zhang, G.; Wang, Z.X.; Hu, B.; Lu, Q. Calcium formate assisted catalytic pyrolysis of pine for enhanced production of monocyclic aromatic hydrocarbons over bimetal-modified HZSM-5. *Bioresour. Technol.* **2020**, *315*, 123805. [CrossRef] [PubMed]
38. Fu, L.; Xiong, Q.; Wang, Q.; Cai, L.; Chen, Z.; Zhou, Y. Catalytic Pyrolysis of Waste Polyethylene Using Combined CaO and Ga/ZSM-5 Catalysts for High Value-Added Aromatics Production. *ACS Sustain. Chem. Eng.* **2022**, *10*, 9612–9623. [CrossRef]

Disclaimer/Publisher's Note: The statements, opinions and data contained in all publications are solely those of the individual author(s) and contributor(s) and not of MDPI and/or the editor(s). MDPI and/or the editor(s) disclaim responsibility for any injury to people or property resulting from any ideas, methods, instructions or products referred to in the content.